iScience

CellPress
OPEN ACCESS

Article

Cellular plasticity and immune microenvironment of malignant pleural effusion are associated with EGFR-TKI resistance in non–small-cell lung carcinoma

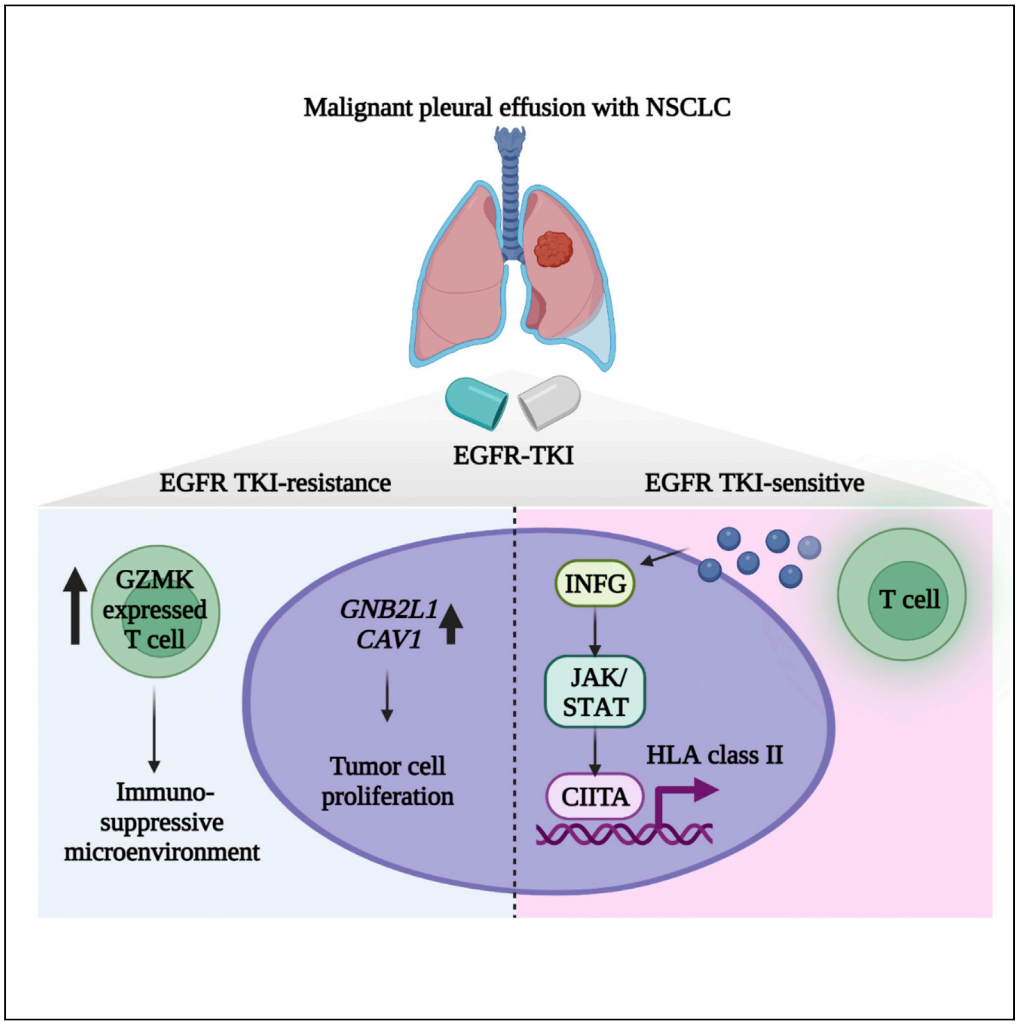

Hyoung-oh Jeong, Hayoon Lee, Hyemin Kim, ..., Keunchil Park, Semin Lee, Se-Hoon Lee

seminlee@unist.ac.kr (S.L.)
shlee119@skku.edu (S.-H.L.)

Highlights

ScRNA-seq reveals associations between cellular plasticity and EGFR-TKI response

Lung epithelial progenitor-like cells are abundant in the TKI-resistant group

HLA-II gene expression are upregulated in the epithelial cells of TKI-sensitive group

Immunosuppressive TME was associated with the TKI resistance in NSCLC

Jeong et al., iScience 25, 105358
November 18, 2022
https://doi.org/10.1016/j.isci.2022.105358

iScience

CellPress
OPEN ACCESS

Article

Cellular plasticity and immune microenvironment of malignant pleural effusion are associated with EGFR-TKI resistance in non–small-cell lung carcinoma

Hyoung-oh Jeong,[1,2,8] Hayoon Lee,[3,4,8] Hyemin Kim,[3,8] Jinho Jang,[1,2] Seunghoon Kim,[1,2] Taejoo Hwang,[1,2] David Whee-Young Choi,[1,2] Hong Sook Kim,[5] Naeun Lee,[6] Yoo Mi Lee,[6] Sehhoon Park,[7] Hyun Ae Jung,[7] Jong-Mu Sun,[7] Jin Seok Ahn,[7] Myung-Ju Ahn,[7] Keunchil Park,[7] Semin Lee,[1,2,*] and Se-Hoon Lee[4,7,9,*]

SUMMARY

Malignant pleural effusion (MPE) is a complication of lung cancer that can be used as an alternative method for tissue sampling because it is generally simple and minimally invasive. Our study evaluated the diagnostic potential of non–small-cell lung carcinoma (NSCLC)-associated MPE in terms of understanding tumor heterogeneity and identifying response factors for EGFR tyrosine kinase inhibitor (TKI) therapy. We performed a single-cell RNA sequencing analysis of 31,743 cells isolated from the MPEs of 9 patients with NSCLC (5 resistant and 4 sensitive to EGFR TKI) with EGFR mutations. Interestingly, lung epithelial precursor-like cells with upregulated *GNB2L1* and *CAV1* expression were enriched in the EGFR TKI-resistant group. Moreover, *GZMK* upregulated transitional effector T cells, and plasmacytoid dendritic cells were significantly enriched in the EGFR TKI-resistant patients. Our results suggest that cellular plasticity and immunosuppressive microenvironment in MPEs are potentially associated with the TKI response of patients with EGFR-mutated NSCLC.

INTRODUCTION

Advanced non-small-cell lung cancer (NSCLC) is the leading cause of cancer-related deaths globally and accounts for 85% of lung cancer cases (Herbst et al., 2008). Patients with epidermal growth factor receptor (EGFR)-mutated NSCLC show sensitivity to EGFR tyrosine kinase inhibitors (TKIs) such as gefitinib, erlotinib, and osimertinib (Riely et al., 2006). However, approximately 10% of patients with EGFR-mutated NSCLC exhibit primary resistance to EGFR TKIs, showing a clinical feature of disease progression during the initial course of EGFR-TKI therapy.

Previous studies on primary resistance to EGFR-TKIs have reported actionable or novel gene alterations with targeted exome sequencing analysis using surgical tumors and biopsy specimens. Representative types of known alterations are as follows: MET amplification (Lai et al., 2019), *de novo* T790M (Su et al., 2018; Zhong et al., 2017), ERBB2 amplification (Zhong et al., 2017), BIM deletion (Lee et al., 2013), PIK3CA mutation (Su et al., 2018), and PTEN mutation (Su et al., 2018; Zhong et al., 2017). Despite various studies, the mechanism of resistance is unknown in up to 50% of cases (Leonetti et al., 2019). Recently, as immunotherapy has emerged, the relationship between the PD-L1 expression and TKI response has also been reported (Su et al., 2018; Takashima et al., 2018), but there have been few studies on the association between TKI resistance and the tumor microenvironment (TME).

Patients with many advanced-stage NSCLC experience malignant pleural effusion (MPE). MPE causes discomfort and pain for the patient and requires additional management, but it can be a resource for the pathologic and genetic analysis of cancer. Basak et al. suggested that MPE is a proper model to investigate intra-tumoral heterogeneity in lung cancer because it incorporates various MPE-fluid component cells, including tumor and stromal cells (Basak et al., 2009). Donnenberg et al. reported several important advantages of MPE, such as an abundant amount of T cells and a proper cross-section of tumor-infiltrating

[1]Department of Biomedical Engineering, Ulsan National Institute of Science and Technology (UNIST), Ulsan, Republic of Korea

[2]Korean Genomics Center, UNIST, Ulsan, Republic of Korea

[3]Medical Research Institute, Sungkyunkwan University School of Medicine, Seoul, Republic of Korea

[4]Department of Health Sciences and Technology, Samsung Advanced Institute of Health Sciences and Technology, Sungkyunkwan University, Seoul, Republic of Korea

[5]Department of Biological Sciences, Sungkyunkwan University, Suwon, Republic of Korea

[6]Samsung Biomedical Research Institute, Samsung Medical Center, Seoul, Republic of Korea

[7]Division of Hematology-Oncology, Department of Medicine, Samsung Medical Center, Sungkyunkwan University School of Medicine, Seoul, Republic of Korea

[8]These authors contributed equally

[9]Lead contact

*Correspondence: seminlee@unist.ac.kr (S.L.), shlee119@skku.edu (S.-H.L.)

https://doi.org/10.1016/j.isci.2022.105358

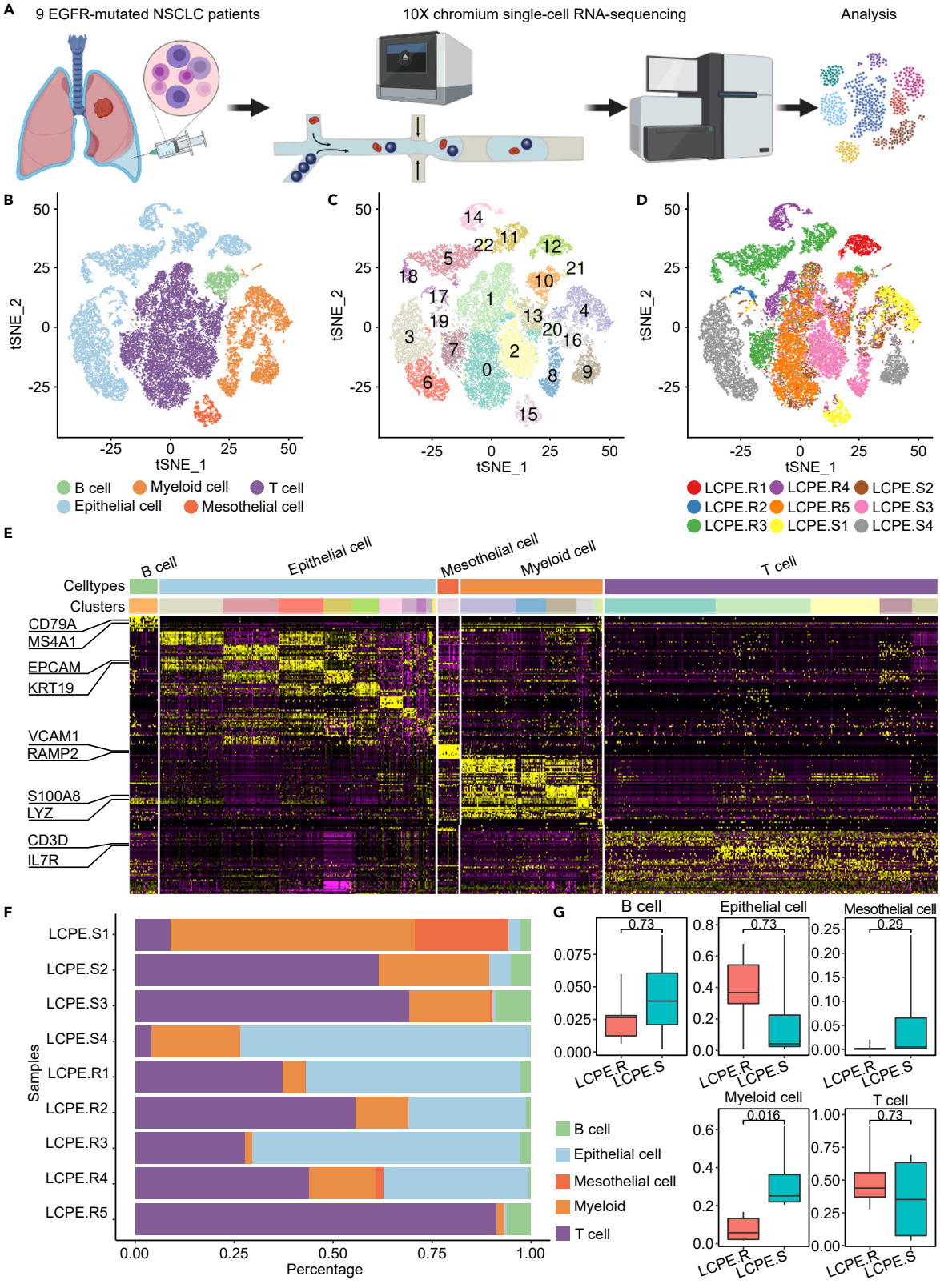
A
9 EGFR-mutated NSCLC patients
10X chromium single-cell RNA-sequencing
Analysis
B
C
D
tSNE_1
tSNE_2
B cell
Myeloid cell
T cell
Epithelial cell
Mesothelial cell
LCPE.R1
LCPE.R2
LCPE.R3
LCPE.R4
LCPE.R5
LCPE.S1
LCPE.S2
LCPE.S3
LCPE.S4
E
Celltypes
Clusters
CD79A
MS4A1
EPCAM
KRT19
VCAM1
RAMP2
S100A8
LYZ
CD3D
IL7R
F
Samples
Percentage
G
B cell
Epithelial cell
Mesothelial cell
Myeloid cell
T cell
0.73
0.73
0.29
0.016
0.73
LCPE.R
LCPE.S

Figure 1. Cell types identified from MPE samples of NSCLC patients using scRNA-seq

(A) The workflow of the overall study design.

(B–D) The t-SNE projection of 31,743 single cells from the MPEs of 9 NSCLC patients shows 5 major cell types, including epithelial, mesothelial, T, B, and myeloid cells. A single cell corresponds to each point, and colors are assigned according to cell type (B), cluster (C), and patient (D).

(E) Heatmap for *Z* score normalized expression profiles of DEGs in each cluster (highlighted genes are known cell markers).

(F) Cell type composition of each patient.

(G) Boxplot for the proportion of major cell types in the resistant and sensitive groups. MPE, malignant pleural effusion; NSCLC, non–small-cell lung carcinoma; t-SNA, t-stochastic neighbor embedding; DEGs, differentially expressed genes.

lymphocytes (TIL) compared with the spatial heterogeneity of TIL in biopsy specimens (Donnenberg et al., 2019).

The development of single-cell RNA sequencing (scRNA-seq) has enabled the analysis of extensive tumor heterogeneity and the identification of various cell populations at the single-cell level. However, the biggest hurdle to scRNA-seq is the limited availability of samples because meticulous preparation procedures are required to separate adherent cells immediately after samples are collected. This limitation prevents the use of cryopreserved tissue samples without labor-intensive immediate cell separation. Hence, most previous scRNA-seq studies on lung cancers have utilized primary and metastatic lesions to understand their cellular features and TME (Guo et al., 2018; Kim et al., 2020; Lambrechts et al., 2018; Maynard et al., 2020). However, cryopreserved pleural effusion with simple pre-freezing preparation can overcome this limitation. Recently, Huang et al. reported that MPEs from patients with NSCLC harbor various types of immune cells such as T and B cells and macrophages, which can provide therapeutic targets and biomarkers for treating NSCLC (Huang et al., 2021). Kashima et al. also utilized a pleural effusion sample from an EGFR-mutated lung cancer patient to validate their findings from the scRNA-seq analysis of TKI resistant cell line models (Kashima et al., 2021).

Here, we sought to establish the TKI response factors with cryopreserved MPEs from patients with EGFR-mutated NSCLC. Transitional effector T cells with high *GZMK* expression and plasmacytoid dendritic cells were significantly enriched in the TKI-resistant group. Furthermore, lung epithelial precursor-like cells were enriched in the EGFR TKI-resistant group, while suprabasal-like cells were more prominent in the sensitive group. In addition, cancer-testis (CT) antigen genes such as *CSAG1* and *MAGEA3*, which are frequently overexpressed in magnoid lung cancer subtypes, were upregulated in the epithelial cells of the TKI-resistant group compared to those in the sensitive one. In contrast, the expression of tumor-specific HLA class II and JAK-STAT pathway genes regulating the HLA class II expression was significantly downregulated in the TKI-resistant group. Overall, we demonstrated that the cellular plasticity of malignant epithelial cells and immune microenvironment are potentially associated with the TKI response of patients with NSCLC.

RESULTS

Single-cell RNA-sequencing analysis from pleural effusion samples of patients with non–small-cell lung carcinoma

We performed a scRNA-seq analysis of 38,414 cells isolated from the MPEs of 9 patients with NSCLC, including 5 EGFR-TKI resistant (LCPE.R) and 4 sensitive patients (LCPE.S) with EGFR mutations (Table S1), to investigate the heterogeneity of cancer cells and the tumor microenvironment (Figure 1A). After quality control, single-cell transcriptome profiles were obtained from a total of 31,743 cells. In addition, doublets were removed from the scRNA-seq datasets of each patient using Scrublet (Wolock et al., 2019), and an average of 4,268 cells per sample was obtained. The observed average number of genes per cell was 1,103, and the average number of unique molecular identifiers (UMIs) per cell was 5,537 (Figures S1A and S1B). To investigate the composition of cell types in MPE, we performed unsupervised graph cluster analysis and identified five major cell types (Figures 1B-1D). Cell types were annotated using SingleR (Aran et al., 2019) and previously known cell type markers (epithelial cells: *EPCAM*, *KRT19*; mesothelial cells: *VCAM1*, *RAMP2*; T cells: *PTPRC*, *CD3D*; B cells: *CD79A*, *MS4A1*; myeloid cells: *S100A8*, *LYZ*; Figure 1E). Unlike immune cells, such as T, myeloid, and B cells, epithelial cells were largely distinguished by individual patients (Figure 1D). The cell-type composition for each patient was heterogeneous (Figures 1F and S1C). In particular, the ratio of myeloid cells was enriched in the EGFR-TKI sensitive group compared to the resistant group ($p = 0.016$, Wilcoxon rank-sum test) (Figure 1G). To investigate whether MPE-derived cells could represent the characteristics of tissue-derived cells (Lambrechts et al., 2018), we performed a co-clustering analysis and confirmed that cells were well clustered by their types rather

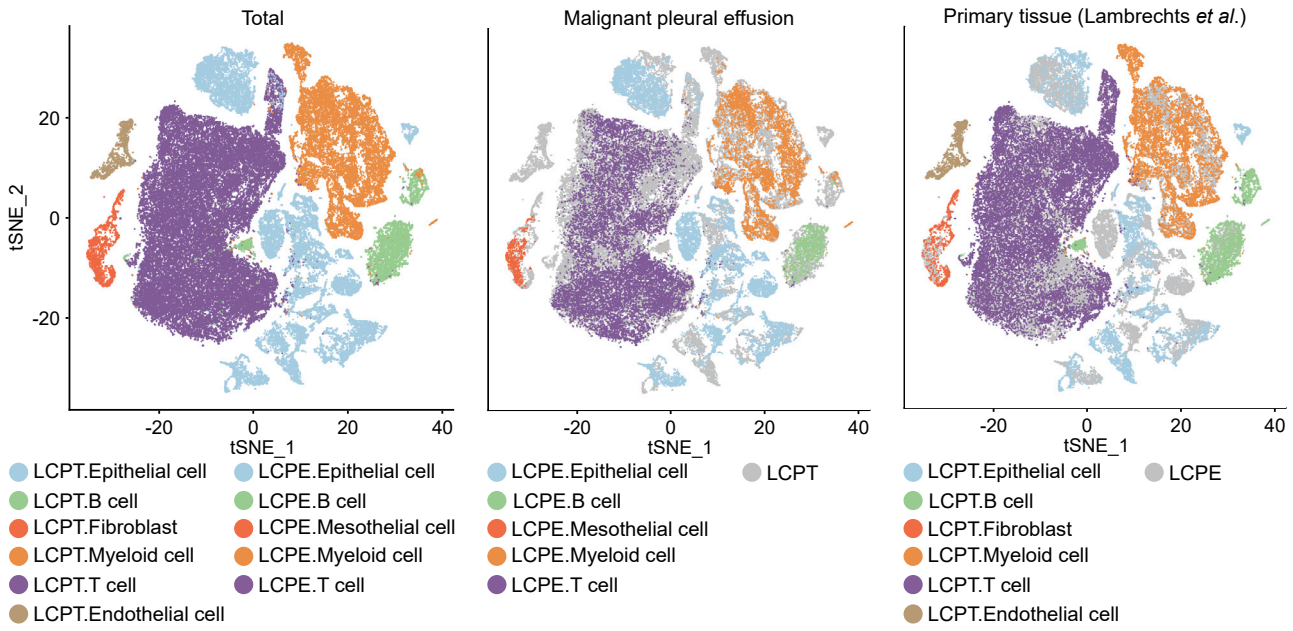

Figure 2. Co-clustering analysis between MPE- and primary tissue-derived cells

Cell type concordance between MPE- and primary tissue-derived cells was confirmed by co-clustering analysis. The color of each dot indicates the cell type, and the gray in the bottom image designates the primary tissue-derived cells (middle) and MPE-derived cells (right), respectively. MPE, malignant pleural effusion.

than their tissue origin (Figure 2). Endothelial cells were observed only from tissue-derived cells and not from MPE. In addition, mesothelial cells from MPE clustered together with fibroblasts from tissue-derived cells.

Tumor heterogeneity conferring tyrosine kinase inhibitor resistance

We performed an additional sub-clustering analysis of epithelial cells at high resolution to further characterize tumor heterogeneity and confirm the differences between the EGFR-TKI resistant and sensitive groups (Figure 3A). As mentioned above, epithelial cells were mainly grouped by individual patients (Figure 3B). We also inferred large-scale chromosomal CNVs in each epithelial cell. The CNV profiles showed significant levels of alterations and heterogeneity, implying that the epithelial cells in MPEs were mostly malignant. In addition, amplification of chr1q and chr7 was recurrently observed in our data, consistent with the previously reported lung adenocarcinoma CNV profiles (Cancer Genome Atlas Research Network, 2014) (Figure 3C).

Additionally, we investigated the expression profiles of a group of genes related to EGFR-TKI resistance and found that *KRAS, ERBB2,* and *IGF1R* were overexpressed in epithelial cells of three TKI-resistant samples (LCPE.R3, LCPE.R4, and LCPE.R5, respectively) (Figure 3D). To validate TKI response based on the above gene expression profiles, we performed drug sensitivity assays using cell cultures derived from LCPE.R4 with *ERBB2* overexpressed and identified considerable sensitivity to afatinib, an irreversible TKI that targets both EGFR and ERBB2 (Wind et al., 2017), and resistance to other TKIs without ERBB2 inhibiting activity (Figure 3E). Taken together, these drug results suggest that the expression of other signaling pathway genes, such as *ERBB2,* can affect TKI resistance.

Cellular plasticity as a mechanism of tyrosine kinase inhibitor resistance

Furthermore, to understand the association between tumor cellular plasticity and EGFR-TKI resistance, we inferred the cellular origins of epithelial cells from MPEs through correlation analysis with previously reported cell types of airway epithelium (Figure S2A) (Deprez et al., 2020). Interestingly, the precursor-like cells were relatively enriched in the resistant group, while the suprabasal-like cells were more prominent in the sensitive group (Figures 3F and 3G). We performed differentially expressed genes (DEG) analysis to determine the characteristics of these two cell types and observed the upregulation of *SCGB3A2*, a club cell

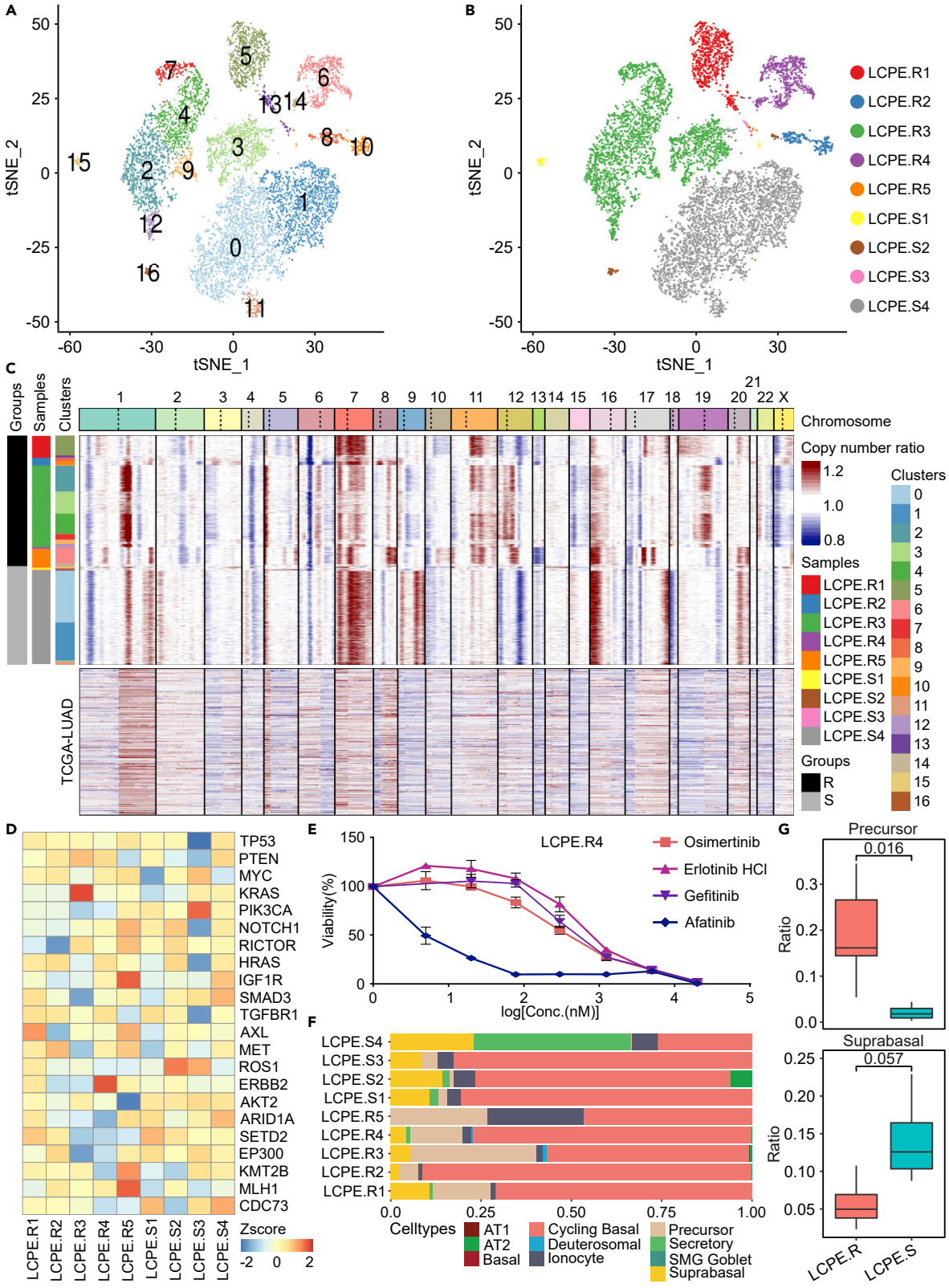
A
B
tSNE_1
tSNE_2
LCPE.R1
LCPE.R2
LCPE.R3
LCPE.R4
LCPE.R5
LCPE.S1
LCPE.S2
LCPE.S3
LCPE.S4
C
Groups
Samples
Clusters
Chromosome
Copy number ratio
Samples
Clusters
Groups
TCGA-LUAD
D
TP53
PTEN
MYC
KRAS
PIK3CA
NOTCH1
RICTOR
HRAS
IGF1R
SMAD3
TGFBR1
AXL
MET
ROS1
ERBB2
AKT2
ARID1A
SETD2
EP300
KMT2B
MLH1
CDC73
Zscore
E
LCPE.R4
Osimertinib
Erlotinib HCl
Gefitinib
Afatinib
Viability(%)
log[Conc.(nM)]
F
Celltypes
AT1
AT2
Basal
Cycling Basal
Deuterosomal
Ionocyte
Precursor
Secretory
SMG Goblet
Suprabasal
G
Precursor
0.016
Suprabasal
0.057
Ratio
LCPE.R
LCPE.S

Figure 3. Heterogeneity of epithelial cells from MPE samples

(A and B) Sub-clusters of MPE-derived epithelial cells from nine NSCLC patients were shown by t-SNE projection, and the color was indicated by cluster (A) and patient (B).

(C) CNV was inferred using gene expression levels of epithelial cells. The top of the heatmap indicates CNVs identified from MPE-derived single cells, and the bottom indicates CNVs of lung adenocarcinoma (LUAD) from The Cancer Genome Atlas (TCGA) project. Red and blue represent copy gain and loss, respectively.

(D) Heatmap for known EGFR-TKI resistance-related genes. The gene expression was normalized by the *Z* score.

(E) EGFR-TKI drug response test for LCPE.R4 using patient-derived cells.

(F) Cell type composition of each patient.

(G) Boxplot for the proportion of epithelial subtypes in the resistant and sensitive groups. MPE, malignant pleural effusion; NSCLC, non–small-cell lung carcinoma; t-SNA, t-stochastic neighbor embedding; CNV, copy number variation; EGFR-TKI, epidermal growth factor receptor-tyrosine kinase inhibitor.

precursor marker (He et al., 2021), in the precursor-like cells (Figure S2B). In addition, genes related to tumor cell proliferation, such as *GNB2L1* and *ZFAS1*, had higher expression levels in the precursor-like cells than other lung epithelial cell subtypes identified in MPEs (Figure S2B) (Duff and Long, 2017; Fan et al., 2020). In contrast, the expression of tumor suppressor genes, including *KLF6* and *RHOB*, was upregulated in the suprabasal-like cells (Figure S2C) (Ito et al., 2004; Mazieres et al., 2004). Through gene set enrichment analysis (GSEA), we found that the Myc targets V1 and TNF-α signaling pathways were enriched in the precursor-like and suprabasal-like cells, respectively (Figure S2D). Interestingly, the expression of MHC class II genes (*HLA-DQB1* and *HLA-DRB5*) was higher in the suprabasal-like cells than that in other epithelial cell subtypes.

Decreased human leukocyte antigen class II expression in epithelial cells of epidermal growth factor receptor-tyrosine kinase inhibitor -resistant and clinical validation

Next, the DEGs of epithelial cells between EGFR-TKI resistant and sensitive patients were analyzed. Epithelial cells of each patient were combined to generate a pseudo-bulk sample for DEG analysis. As a result, we identified 673 upregulated and 628 downregulated genes in the EGFR-TKI-resistant group compared with the sensitive group ($p < 0.05$ and absolute fold-change > 1.5). According to a previous large-scale multi-omics study of lung adenocarcinoma by The Cancer Genome Atlas project, EGFR-mutant lung adenocarcinoma mostly belongs to the bronchial subtype (Cancer Genome Atlas Research Network, 2014). Interestingly, *CSAG1* and *MAGEA3*, known as cancer-testis (CT) genes, were upregulated in the epithelial cells of the resistant group (Figure 4A); previous studies have shown that these genes are most frequently activated in the magnoid subtype of lung adenocarcinoma (Yao et al., 2014). Hence, the expression profiles of magnoid subtype-related genes could be associated with resistance to the EGFR-TKI therapy.

Through GSEA, we found that the downregulated genes in the epithelial cells of the resistant group were associated with the immune response (Figure 4B). In particular, *HLA-DPB1*, *HLA-DQA1*, and *HLA-DRB1* showed significantly lower expression levels in the resistant group than those in the sensitive group (Figures 4C and S3A), which is concordant with the DEG analysis results between lung epithelial precursor-like and suprabasal-like cells. To verify our findings, we examined whether HLA class II genes were expressed in the published human lung cancer scRNA-seq data (Lambrechts et al., 2018). As a result, most HLA class II genes were highly expressed in immune cells, such as T, myeloid, and B cells, but some HLA class II genes were also highly expressed in epithelial cells (Figure S3B). Regulation of MHC class II expression is known to be mediated by the transactivator gene *CIITA* and induced by *IFNG* (Steimle et al., 1994). Although there was no apparent difference in the expression levels of *IFNG* between the two groups, the expression of *CIITA* was increased in the EGFR-TKI sensitive group (Figure S3C). To gain deeper insights into the causes of the difference in the HLA class II gene expression levels, we investigated the upstream JAK-STAT signaling pathway genes regulating HLA class II genes. Interestingly, we found that the expression levels of JAK-STAT signaling pathway-related genes tended to increase in the EGFR-TKI sensitive group (Figure S3C). By adopting a scoring scheme for JAK-STAT pathway activity, we confirmed that the JAK-STAT pathway was significantly activated in the sensitive group ($p = 0.032$) (Figure 4D).

To validate the distinct expression patterns of the three MHC class II proteins in the epithelial cells of the primary tumor, formalin-fixed and paraffin-embedded (FFPE) slides for 19 TKI-resistant and 45 TKI-sensitive patients underwent immunohistochemistry (IHC) staining (Figures 4E and S3D). The IHC scores of HLA-DPB1 ($p = 0.001$) and HLA-DRB1 ($p = 0.007$) were significantly lower in the TKI-resistant group (Figure 4F). Although there was no statistical significance ($p = 0.2$), the IHC score of HLA-DQA1 was also lower in the resistant group. Moreover, PFS was significantly better in patients with high (median IHC score HLA-DPB1 240, HLA-DQA1 30, HLA-DRB1 35) MHC class II expression than those with low MHC class II expression

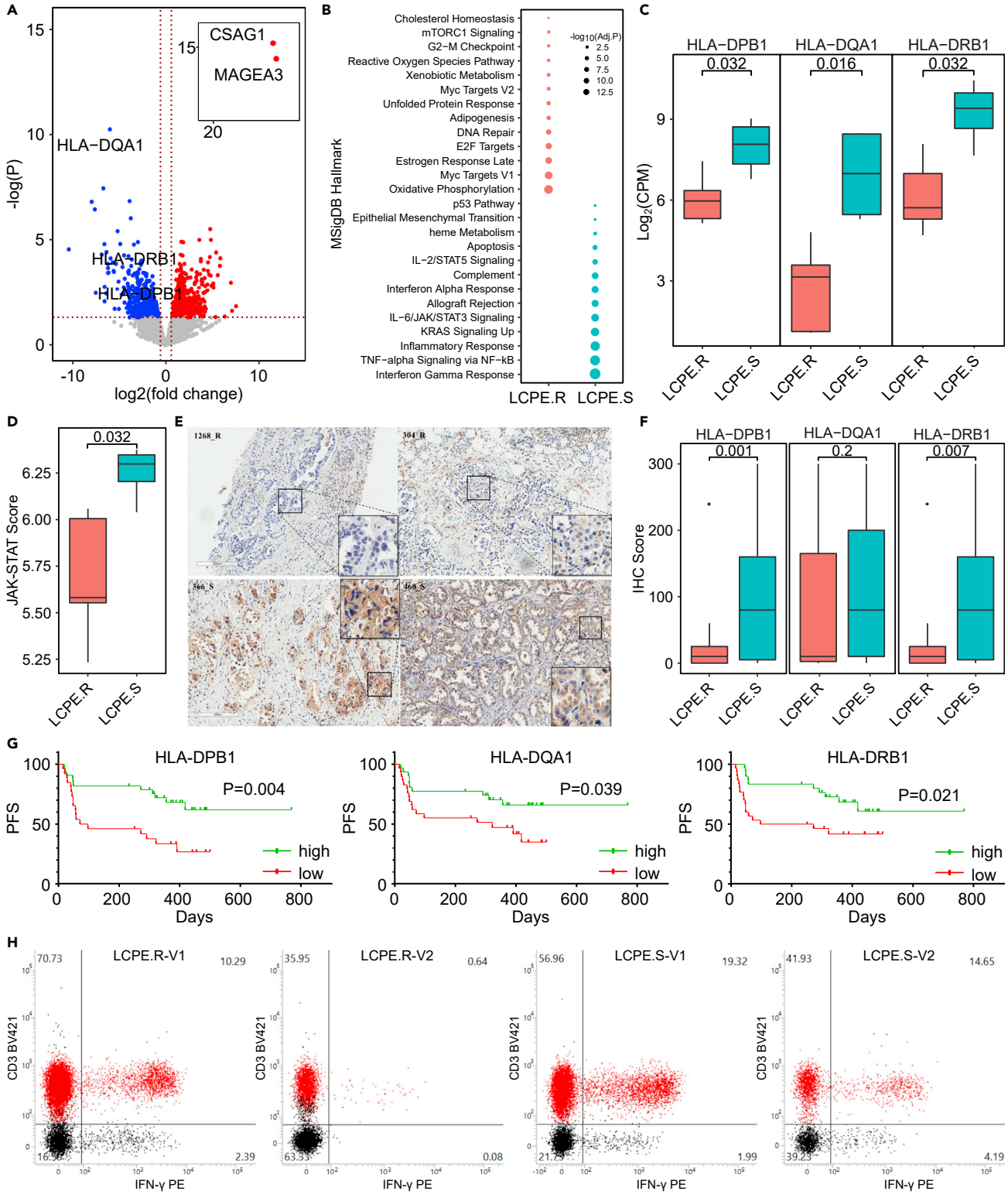

Figure 4. Clinical validation of HLA class II expression based on TKI response

(A) Volcano plot for pseudo-bulk-based DEGs between the resistant and sensitive groups. Red and blue dots represent upregulated genes in the resistant and sensitive groups, respectively.

(B) The resistant group's enriched gene ontology terms were illustrated in red, whereas the sensitive group's enriched gene ontology terms were shown in blue.

Figure 4. *Continued*

(C) Comparison of HLA class II (*HLA-DPB1*, *HLA-DQA1*, and *HLA-DRB1*) expression between the TKI resistant (LCPE.R) and sensitive (LCPE.S) groups (Wilcoxon rank-sum test).

(D) Boxplot for the comparison of JAK-STAT score between the resistant and sensitive groups ($p = 0.032$, Wilcoxon rank-sum test).

(E) IHC staining of MHC class II in the two resistant (top) and two sensitive patient samples (bottom). 100× magnification and 200× partial magnification with a lattice length of 125 μm.

(F) Boxplot for the comparison of IHC scores based on MHC class II (HLA-DPB1, HLA-DQA1, and HLA-DRB1) expression between the resistant and sensitive groups.

(G) Survival plot showing PFS dependence on high and low HLA-DPB1 (HR 2.837, 95% CI 1.333-6.041), HLA-DQA1 (HR 2.219, 95% CI 1.036-4.749), and HLA-DRB1 (HR 2.417, 95% CI 1.123-5.199) subtype expression.

(H) Flow cytometry analysis of interferon (IFN)-γ producing MPE cells from the two EGFR-TKI resistant (left) and two sensitive patient samples (right). TKI, tyrosine kinase inhibitor; DEGs, differentially expressed genes; IHC, immunohistochemistry; PFS, progression-free survival.

(Figure 4G). The expression levels of MAGEA3, CSAG1, CIITA and HLA-DR in MPE-derived epithelial cells were further validated using multiplex immunofluorescence staining, which showed increased MAGEA3 and CSAG1 as well as decreased CIITA and HLA-DR in TKI-resistant group (Figures S4A and S4B). We verified that HLA-DR$^+$ epithelial cells were increased in the EGFR-TKI sensitive group through flow cytometry analysis (Figures S4C and S4D). In addition, HLA-DR and HLA-DQ were notably upregulated in EGFR-TKI sensitive MPE cells (Figures S4E). To confirm the expression of IFN-γ in the tumor microenvironment, IFN-γ-producing CD3$^+$ cells after PMA and ionomycin stimulation were higher in TKI-sensitive MPEs than in TKI-resistant MPEs (Figure 4H).

Enrichment of transitional effector T cells in epidermal growth factor receptor-tyrosine kinase inhibitor resistant patients

We performed a co-clustering analysis of T cells from primary tumors (Lambrechts et al., 2018) and MPEs. Nine helper T cell clusters were characterized by the expression of *CD4*, *CCR4*, *CCR6*, and *IL6R*; two dysfunctional T cell clusters by *CD8A*, *LAG3*, and *PDCD1* expression; three transitional effector T cell clusters by dysfunctional T cell marker gene and *GZMK* expression; two natural killer (NK) cell clusters by *CD3D*, *CD160*, *NCR3*, *CX3CR1*, and *FGFBP2* expression; one naive T cell cluster by *SELL*, *TCF7*, *CCR7*, and *LEF1* expression; and one regulatory T cell (Treg) cluster by *FOXP3*, *IL2RA*, *TNFRSF4*, *TIGIT*, and *CTLA4* expression (Figures 5A-5D). Overall, the T cell subtypes were heterogeneously distributed across the individual patients (Figure S5A). Most of the T cell clusters were identified from both primary tumors and MPEs without significant differences in their enrichment level (Figure S5B) except for clusters 4 (Treg), 10 (helper T cell), 12 (transitional T cell), and 16 (proliferating T cell).

Interestingly, among three transitional effector T cell clusters (clusters 2, 3, and 12), cluster 3 was significantly enriched in the TKI-resistant group ($p = 0.032$, Wilcoxon rank-sum test) (Figures 5E and S5C), and the expression of *GZMK* and *FYN* was higher than that of the other clusters. *FYN* is known to phosphorylate the negative regulator of T cell signaling and may be involved in terminating the TCR signal (Filby et al., 2007).

Heterogeneity of myeloid cells in pleural effusion samples

We identified nine macrophage clusters, one non-classical monocyte cluster, one myeloid precursor cluster, one classical dendritic cell cluster, one activated dendritic cell cluster, and one plasmacytoid dendritic cell (pDC) cluster (Figures 6A–6D). Similar to T cell subtypes, myeloid cell subtypes were also heterogeneously distributed across the individual patients (Figure S6A). Most of the myeloid cell clusters were identified from both primary tumors and MPEs without significant differences in their enrichment level, except for clusters 0 (macrophage), 10 (activated dendritic cell), 13 (macrophage), and 14 (pDC) (Figure S6B). Myeloid precursor and pDC clusters were enriched in the TKI-resistant group (Figures 6E and S6C). The pDC cluster (cluster 14) with high granzyme B (*GZMB*) expression is known to induce regulatory T cell response (Swiecki and Colonna, 2015) and to inhibit T cell proliferation (Jahrsdorfer et al., 2010). The myeloid precursor cluster (cluster 11) had a high expression of genes associated with cell cycles such as *CCNB1*, *CCNB2*, *CDC20*, and *CDK1* (Engeland, 2018).

DISCUSSION

Most NSCLC patients with EGFR mutations are responsive to EGFR-TKI therapy, but approximately 10% of patients show primary resistance to TKI (Lee et al., 2013; Sharma et al., 2007). Recent studies have suggested that MPE is an appropriate model for investigating the heterogeneity and the immune microenvironment of lung cancer because MPE preserves tumor, stromal, and immune cells (Basak et al.,

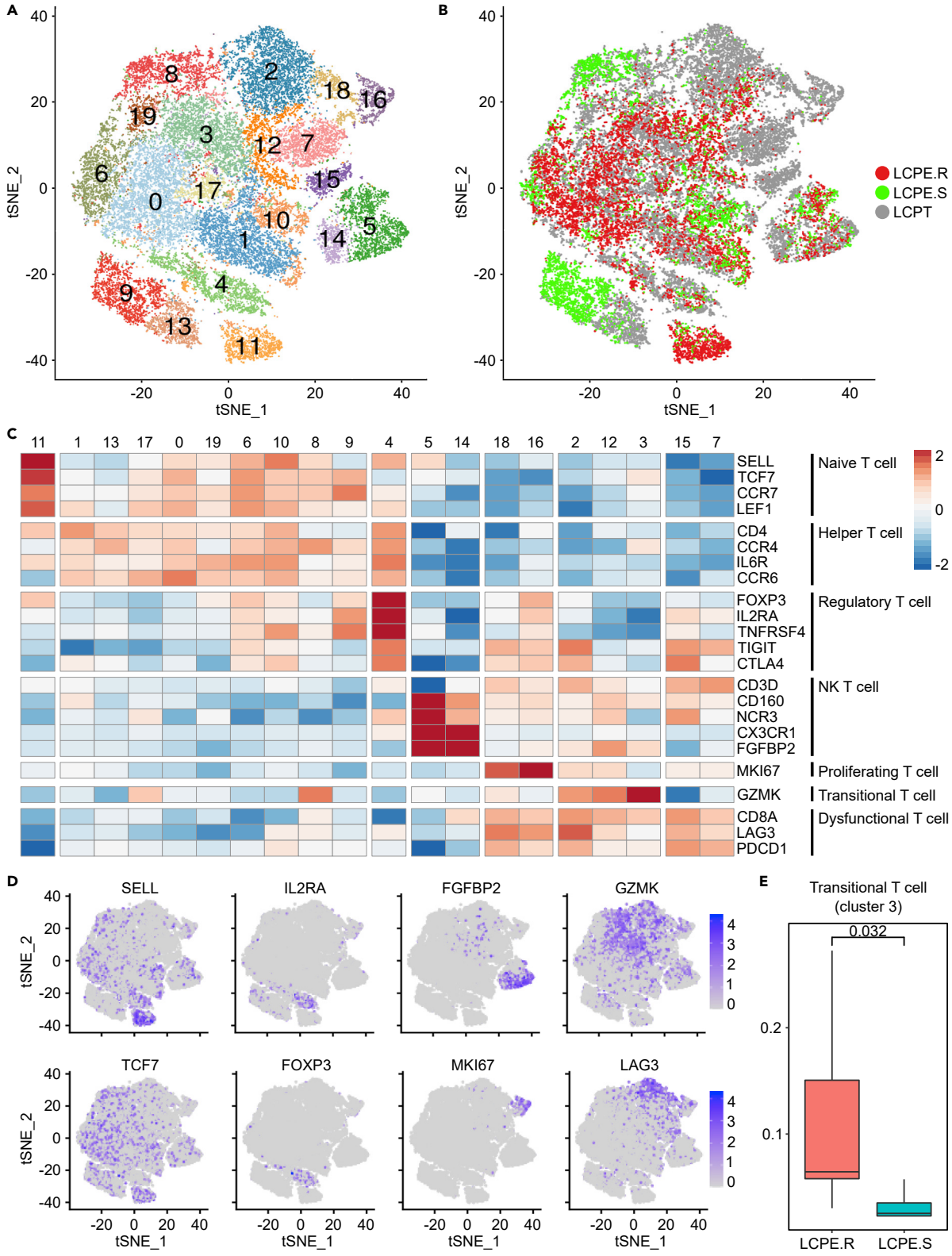
A
B
tSNE_1
tSNE_2
LCPE.R
LCPE.S
LCPT
C
SELL
TCF7
CCR7
LEF1
CD4
CCR4
IL6R
CCR6
FOXP3
IL2RA
TNFRSF4
TIGIT
CTLA4
CD3D
CD160
NCR3
CX3CR1
FGFBP2
MKI67
GZMK
CD8A
LAG3
PDCD1
Naive T cell
Helper T cell
Regulatory T cell
NK T cell
Proliferating T cell
Transitional T cell
Dysfunctional T cell
D
SELL
IL2RA
FGFBP2
GZMK
TCF7
FOXP3
MKI67
LAG3
E
Transitional T cell
(cluster 3)
0.032
LCPE.R
LCPE.S

Figure 5. Clustering of MPE-derived T cells in NSCLC patients

(A) Co-clustering of MPE-derived T cells from nine NSCLC patients and primary tissue-derived T cells was shown by t-SNE projection. The color of each dot indicates a cluster.

(B) The T cells derived from the primary tissue, the resistant and sensitive groups are plotted in gray, red, and green, respectively.

(C) Heatmap for *z*-score-normalized expression profiles of known T cell subtype marker genes in each cluster.

(D) t-SNE plots showing expression of T cell subtype marker genes.

(E) Boxplot for the proportion of transitional T cells (cluster 3) in the resistant and sensitive groups ($p = 0.032$, Wilcoxon rank-sum test). MPE, malignant pleural effusion; NSCLC, non–small-cell lung carcinoma; t-SNA, t-stochastic neighbor embedding.

2009; Huang et al., 2021; Maynard et al., 2020), and its sampling is minimally invasive. Despite having these advantages, most single-cell analyses of NSCLC have been based on tumors (Guo et al., 2018; Kim et al., 2020; Lambrechts et al., 2018), and MPE has rarely been utilized. To the best of our knowledge, we are the first to analyze the cellular landscapes potentially associated with EGFR-TKI response at the single-cell level using MPEs of NSCLC patients with EGFR mutations.

We examined the expression of 22 genes known to be associated with EGFR-TKI response in epithelial cells from MPE (Table S2). A drug response test was further conducted on the cell culture from the TKI-resistant sample (LCPE.R4) with *ERBB2* upregulation, and interestingly, it showed sensitivity to afatinib, a dual-targeting drug of ERBB2 and EGFR (Figure 3D). Unfortunately, in actual clinical practice, the patient from which the LCPE.R4 MPE cell culture was obtained did not receive afatinib treatment because there was no such data at the time, and it is expected that if he had received the treatment, he would have benefited.

The major drug resistance factors can be divided into genetic mutagenicity and non-mutagenic mechanisms. The non-mutagenic mechanism is mainly caused by cellular plasticity and is closely related to the re-activation of developmental programs such as cancer stem cell characteristics and the epithelial-mesenchymal transition (Qin et al., 2020). Therefore, we examined the relationship between cellular plasticity and TKI resistance through single-cell transcriptome analysis of MPEs from TKI-resistant and -sensitive patients with EGFR mutations. Our results showed that precursor-like and suprabasal-like cells were enriched in the resistant and sensitive groups, respectively. In the precursor-like cells, genes related to tumor cell proliferation (*GNB2L1*, *CAV1*, and *ZFAS1*) were generally upregulated. *GNB2L1* is known to promote tumor cell proliferation by regulating Src activity (Duff and Long, 2017; Peng et al., 2013). In addition, *GNB2L1* and Src regulate P-glycoprotein activity by caveolin-1 (*CAV1*) phosphorylation (Fan et al., 2019). P-glycoprotein, a drug transporter in cancer cells, is one of the main causes of multidrug resistance because it helps excrete anticancer drugs out of the cell (Fan et al., 2019). *ZFAS1* induces tumor cell proliferation and migration by directly binding with miR-1271-5p, which acts as a tumor suppressor in lung adenocarcinoma (Fan et al., 2020). Maynard et al. analyzed advanced-stage NSCLC patients with EGFR mutations using a scRNA-seq technique and demonstrated that residual tumor cells during therapy had enhanced alveolar cell signatures, and tumor cells that acquired resistance reduced immunity (Maynard et al., 2020). According to them, *CAV1* is upregulated in treatment-resistant tumor cells and transcriptionally activates the WNT/β-catenin pathway. They also suggested that the activation of the WNT/β-catenin pathway in NSCLC patients with EGFR mutations may lead to resistance to EGFR inhibitors (Maynard et al., 2020). Although very few alveolar cells were identified in our results (Figure 3F), *CAV1* was significantly upregulated in the precursor-like cells that were abundant in the TKI-resistant group (Figures 3G and S2B), which is concordant with the results from Maynard et al. The suprabasal-like cells, which accounted for a high cellular proportion in the sensitive group, showed upregulation of *KLF6*, *RHOB*, *HLA-DQB1*, and *HLA-DRB5*. The KLF family is known to be involved in cell differentiation, proliferation, and apoptosis (Black et al., 2001). Among them, *KLF6* is frequently downregulated in NSCLC and inhibits tumor cell growth by inducing apoptosis (Ito et al., 2004). Reduction of *RHOB* expression often occurs in lung cancer and enhances tumor suppressive activity (Mazieres et al., 2004). Taken together, both proliferative properties and increased expression of drug transporter genes in precursor-like cells are associated with TKI resistance.

We also found that some immune response-related genes are downregulated in the TKI-resistant group (Figure 4B). In particular, the expression of HLA class II genes was significantly reduced in the epithelial cells of the TKI-resistant group. In general, HLA class II is known to be expressed in professional antigen-presenting cells (APCs), but recent studies have confirmed the expression of HLA class II from non-professional APCs, including epithelial cells (Axelrod et al., 2019; Wosen et al., 2018). In the tumor microenvironment, the MHC class II-mediated antigen presentation of epithelial cells appears to play an important role in

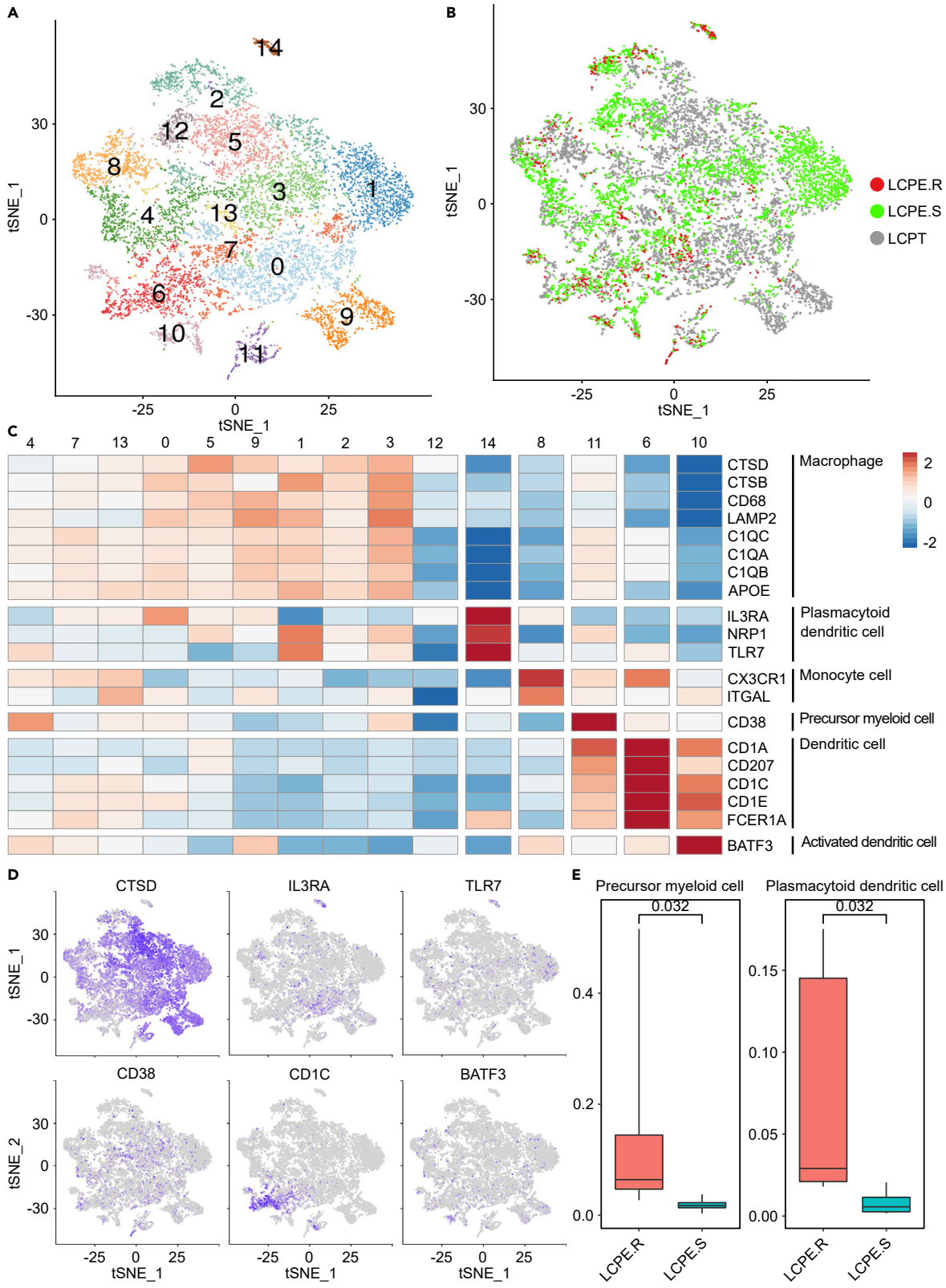
A
B
C
D
E
tSNE_1
tSNE_2
LCPE.R
LCPE.S
LCPT
CTSD
CTSB
CD68
LAMP2
C1QC
C1QA
C1QB
APOE
IL3RA
NRP1
TLR7
CX3CR1
ITGAL
CD38
CD1A
CD207
CD1C
CD1E
FCER1A
BATF3
Macrophage
Plasmacytoid dendritic cell
Monocyte cell
Precursor myeloid cell
Dendritic cell
Activated dendritic cell
Precursor myeloid cell
Plasmacytoid dendritic cell
0.032
0.032

Figure 6. Clustering of MPE-derived myeloid cells in NSCLC patients

(A) Co-clustering of MPE-derived myeloid cells from nine NSCLC patients and primary tissue-derived myeloid cells was shown by t-SNE projection. The color of each dot indicates a cluster.

(B) The myeloid cells derived from the primary tissue, the resistant and sensitive groups are plotted in gray, red, and green, respectively.

(C) Heatmap for *z*-score-normalized expression profiles of known myeloid cell subtype marker genes in each cluster.

(D) t-SNE plots showing expression of myeloid cell subtype marker genes.

(E) Boxplot for the proportion of precursor myeloid cells and pDC in the resistant and sensitive groups ($p = 0.032$, Wilcoxon rank-sum test). MPE, malignant pleural effusion; NSCLC, non–small-cell lung carcinoma; t-SNA, t-stochastic neighbor embedding; pDC, plasmacytoid dendritic cells.

regulating the inflammatory response by activating T cells (Mehrfeld et al., 2018). MHC class II expression in the epithelial cells was further confirmed by IHC staining, and notably, patients with high MHC class II expression showed significantly superior EGFR-TKI therapy outcomes (Figures 4E-4G). Therefore, we hypothesized that the difference in HLA class II expression was due to a specific transcription factor and revealed that *CIITA* expression, an HLA class II transcription factor (Devaiah and Singer, 2013), was significantly decreased in the TKI-resistant group. Furthermore, Pollack et al. (2011) reported that *IFNG* activates *CIITA* expression and, subsequently, HLA class II expression. The resistant group exhibited decreased expression of genes related to the IFNG signaling pathway, including *JAK* and *STAT*.

DEG analysis of epithelial cells revealed significant upregulation of *CSAG1* and *MAGEA3* in the resistant group. CT genes such as *CSAG* and *MAGEA* are known potential targets for immunotherapy because they are expressed in various malignant tumors, including lung cancer (Yao et al., 2014). Yao et al. investigated CT gene expression in 10 common cancer types from TCGA and reported that *MAGE* and *CSAG* are activated in the magnoid subtype of lung adenocarcinomas (Yao et al., 2014). Although most of the EGFR-mutated lung adenocarcinomas are the bronchial subtype (Cancer Genome Atlas Research Network, 2014), our analysis showed that some EGFR-TKI resistant patients could have magnoid subtype characteristics (Figure 4A).

Furthermore, transitional effector T cells were more enriched in the TKI-resistant group compared with the sensitive group. Li et al. found that the dysfunction of $CD8^+$ T cells is associated with tumor reactivity and characterized transitional effector T cells in between early effector T cells and dysfunctional T cells (Li et al., 2019). In our data, one transitional effector T cell cluster with a high expression of *FYN*, which activates negative regulators of T cell signaling and is involved in terminating TCR signaling (Filby et al., 2007), was enriched in the TKI-resistant group. We also confirmed that a pDC cluster was enriched in the TKI-resistant group. pDC secretes soluble factors that play an important role in anti-tumor immunity, but inactivated pDC is known to be associated with immunosuppression (Demoulin et al., 2013). Furthermore, the pDC cluster (cluster 14) had a high *GZMB* expression, which induces regulatory T cell responses and inhibits T cell proliferation (Jahrsdorfer et al., 2010; Swiecki and Colonna, 2015). In addition, a previous study reported that an unstimulated pDC expresses *GZMB* and induces regulatory T cell responses (Ye et al., 2020).

Limitations of the study

We investigated EGFR-TKI resistance mechanisms in NSCLC using the limited number of MPE samples. In addition, EGFR-TKI resistant MPE specimens were collected after different types of EGFR-TKI treatments. Therefore, these might influence our interpretation of the results. Furthermore, endothelial cells and fibroblasts, which were not observed in our data, could also potentially affect EGFR-TKI responsiveness. Hence, it will be important in the future to validate in an independent cohort with samples before and after treatment.

STAR★METHODS

Detailed methods are provided in the online version of this paper and include the following:

- KEY RESOURCES TABLE
- RESOURCE AVAILABILITY
  - Lead contact
  - Materials availability
  - Data and code availability
- EXPERIMENTAL MODEL AND SUBJECT DETAILS
  - Collection and preparation of pleural effusion samples of NSCLC patients
- METHOD DETAILS
  - scRNA-seq data processing
  - Correlation analysis of epithelial cells for infer cellular plasticity

- Differential gene expression analysis of pseudo-bulks
- Copy number variation analysis in scRNA-seq
- Cell viability test
- Immunohistochemistry staining
- Multiplex immunofluorescence
- Flow cytometry
- MPE-derived organoid culture
- Analysis of clinical validation cohort

- QUANTIFICATION AND STATISTICAL ANALYSIS

SUPPLEMENTAL INFORMATION

Supplemental information can be found online at https://doi.org/10.1016/j.isci.2022.105358.

ACKNOWLEDGMENTS

We thank the patients who participated in this study and also thank Binnari Kim for the pathological evaluation of the patient samples. This research was supported by Basic Science Research Program through the National Research Foundation of Korea (NRF) funded by the Ministry of Education (NRF-2018R1A6A1A03025810, NRF-2019R1A6A3A13096060, NRF-2021R1I1A1A01052346 and NRF-2021R1I1A1A01052346); supported by the NRF grants funded by the Ministry of Science and ICT (NRF-2017M3C9A5031004, NRF-2021R1A2C1094009 and NRF-2020R1A2C3006535); supported by a grant of the Korea Health Technology R&D Project through the Korea Health Industry Development Institute (KHIDI), funded by the Ministry of Health & Welfare, Republic of Korea (grant number: HR20C0025); supported by Future Medicine 20*30 Project of the Samsung Medical Center (SMX1220091); supported by Ulsan National Institute of Science and Technology (UNIST) R&D Program (2.200566.01) funded by Clinomics Inc.

AUTHOR CONTRIBUTIONS

S.H.L. and S.M.L. conceived this project. H.Y.L. and H.M.K performed biological experiments and clinical data analysis under the supervision of S.H.L.. H.O.J. performed bioinformatics analysis under the supervision of S.M.L.. H.O.J., H.Y.L., S.M.L. and S.H.L. wrote the article, with feedback from J.H.J., S.H.K., T.J.H., D.W.C., H.S.K., H.M.K., N.E.L., Y.M.L., S.P., H.A.J., J.S., J.S.A., M.J.A. and K.P.

DECLARATION OF INTERESTS

JS Ahn reports personal fees from Amgen, Pfizer, AstraZeneca, Menarini, Roche, Eisai, Boehringer Ingelheim, BMSOno, MSD, Janssen, Samsung Bioepis, outside the submitted work. S.H.L. reports grants and personal fees from MSD, personal fees from Novartis, AstraZeneca, BMS, Roche, outside the submitted work. K Park reports personal fees from Astellas, Astra Zeneca, AMGEN, BluePrint, BMS, Boehringer Ingelheim, Daiichi Sankyo, Eisai, Eli Lilly, Merck KGaA, MSD, Novartis, ONO, Puma Biotechnology, Roche, outside the submitted work.

Received: January 18, 2022
Revised: August 24, 2022
Accepted: October 10, 2022
Published: November 18, 2022

REFERENCES

Aran, D., Looney, A.P., Liu, L., Wu, E., Fong, V., Hsu, A., Chak, S., Naikawadi, R.P., Wolters, P.J., Abate, A.R., et al. (2019). Reference-based analysis of lung single-cell sequencing reveals a transitional profibrotic macrophage. Nat. Immunol. *20*, 163–172. https://doi.org/10.1038/s41590-018-0276-y.

Axelrod, M.L., Cook, R.S., Johnson, D.B., and Balko, J.M. (2019). Biological consequences of MHC-II expression by tumor cells in cancer. Clin. Cancer Res. *25*, 2392–2402. https://doi.org/10.1158/1078-0432.CCR-18-3200.

Basak, S.K., Veena, M.S., Oh, S., Huang, G., Srivatsan, E., Huang, M., Sharma, S., and Batra, R.K. (2009). The malignant pleural effusion as a model to investigate intratumoral heterogeneity in lung cancer. PLoS One *4*, e5884. https://doi.org/10.1371/journal.pone.0005884.

Black, A.R., Black, J.D., and Azizkhan-Clifford, J. (2001). Sp1 and kruppel-like factor family of transcription factors in cell growth regulation and cancer. J. Cell. Physiol. *188*, 143–160. https://doi.org/10.1002/jcp.1111.

Butler, A., Hoffman, P., Smibert, P., Papalexi, E., and Satija, R. (2018). Integrating single-cell transcriptomic data across different conditions, technologies, and species. Nat. Biotechnol. *36*, 411–420. https://doi.org/10.1038/nbt.4096.

Cancer Genome Atlas Research Network (2014). Comprehensive molecular profiling of lung adenocarcinoma. Nature *511*, 543–550. https://doi.org/10.1038/nature13385.

Chen, E.Y., Tan, C.M., Kou, Y., Duan, Q., Wang, Z., Meirelles, G.V., Clark, N.R., and Ma'ayan, A.

(2013). Enrichr: interactive and collaborative HTML5 gene list enrichment analysis tool. BMC Bioinf. *14*, 128. https://doi.org/10.1186/1471-2105-14-128.

Demoulin, S., Herfs, M., Delvenne, P., and Hubert, P. (2013). Tumor microenvironment converts plasmacytoid dendritic cells into immunosuppressive/tolerogenic cells: insight into the molecular mechanisms. J. Leukoc. Biol. *93*, 343–352. https://doi.org/10.1189/jlb.0812397.

Deprez, M., Zaragosi, L.E., Truchi, M., Becavin, C., Ruiz García, S., Arguel, M.J., Plaisant, M., Magnone, V., Lebrigand, K., Abelanet, S., et al. (2020). A single-cell atlas of the human healthy airways. Am. J. Respir. Crit. Care Med. *202*, 1636–1645. https://doi.org/10.1164/rccm.201911-2199OC.

Devaiah, B.N., and Singer, D.S. (2013). CIITA and its dual roles in MHC gene transcription. Front. Immunol. *4*, 476. https://doi.org/10.3389/fimmu.2013.00476.

Donnenberg, A.D., Luketich, J.D., Dhupar, R., and Donnenberg, V.S. (2019). Treatment of malignant pleural effusions: the case for localized immunotherapy. J. Immunother. Cancer *7*, 110. https://doi.org/10.1186/s40425-019-0590-4.

Duff, D., and Long, A. (2017). Roles for RACK1 in cancer cell migration and invasion. Cell. Signal. *35*, 250–255. https://doi.org/10.1016/j.cellsig.2017.03.005.

Engeland, K. (2018). Cell cycle arrest through indirect transcriptional repression by p53: I have a DREAM. Cell Death Differ. *25*, 114–132. https://doi.org/10.1038/cdd.2017.172.

Fan, G., Jiao, J., Shen, F., and Chu, F. (2020). Upregulation of lncRNA ZFAS1 promotes lung adenocarcinoma progression by sponging miR-1271-5p and upregulating FRS2. Thorac. Cancer *11*, 2178–2187. https://doi.org/10.1111/1759-7714.13525.

Fan, Y., Si, W., Ji, W., Wang, Z., Gao, Z., Tian, R., Song, W., Zhang, H., Niu, R., and Zhang, F. (2019). Rack1 mediates Src binding to drug transporter P-glycoprotein and modulates its activity through regulating Caveolin-1 phosphorylation in breast cancer cells. Cell Death Dis. *10*, 394. https://doi.org/10.1038/s41419-019-1633-y.

Filby, A., Seddon, B., Kleczkowska, J., Salmond, R., Tomlinson, P., Smida, M., Lindquist, J.A., Schraven, B., and Zamoyska, R. (2007). Fyn regulates the duration of TCR engagement needed for commitment to effector function. J. Immunol. *179*, 4635–4644. https://doi.org/10.4049/jimmunol.179.7.4635.

Guo, X., Zhang, Y., Zheng, L., Zheng, C., Song, J., Zhang, Q., Kang, B., Liu, Z., Jin, L., Xing, R., et al. (2018). Global characterization of T cells in non-small-cell lung cancer by single-cell sequencing. Nat. Med. *24*, 978–985. https://doi.org/10.1038/s41591-018-0045-3.

He, D., Wang, D., Lu, P., Yang, N., Xue, Z., Zhu, X., Zhang, P., and Fan, G. (2021). Single-cell RNA sequencing reveals heterogeneous tumor and immune cell populations in early-stage lung adenocarcinomas harboring EGFR mutations. Oncogene *40*, 355–368. https://doi.org/10.1038/s41388-020-01528-0.

Herbst, R.S., Heymach, J.V., and Lippman, S.M. (2008). Lung cancer. N. Engl. J. Med. *359*, 1367–1380. https://doi.org/10.1056/NEJMra0802714.

Huang, Z.Y., Shao, M.M., Zhang, J.C., Yi, F.S., Du, J., Zhou, Q., Wu, F.Y., Li, S., Li, W., Huang, X.Z., et al. (2021). Single-cell analysis of diverse immune phenotypes in malignant pleural effusion. Nat. Commun. *12*, 6690. https://doi.org/10.1038/s41467-021-27026-9.

Ito, G., Uchiyama, M., Kondo, M., Mori, S., Usami, N., Maeda, O., Kawabe, T., Hasegawa, Y., Shimokata, K., and Sekido, Y. (2004). Kruppel-like factor 6 is frequently down-regulated and induces apoptosis in non-small cell lung cancer cells. Cancer Res. *64*, 3838–3843. https://doi.org/10.1158/0008-5472.CAN-04-0185.

Jahrsdörfer, B., Vollmer, A., Blackwell, S.E., Maier, J., Sontheimer, K., Beyer, T., Mandel, B., Lunov, O., Tron, K., Nienhaus, G.U., et al. (2010). Granzyme B produced by human plasmacytoid dendritic cells suppresses T-cell expansion. Blood *115*, 1156–1165. https://doi.org/10.1182/blood-2009-07-235382.

Kashima, Y., Shibahara, D., Suzuki, A., Muto, K., Kobayashi, I.S., Plotnick, D., Udagawa, H., Izumi, H., Shibata, Y., Tanaka, K., et al. (2021). Single-cell analyses reveal diverse mechanisms of resistance to EGFR tyrosine kinase inhibitors in lung cancer. Cancer Res. *81*, 4835–4848. https://doi.org/10.1158/0008-5472.CAN-20-2811.

Kim, N., Kim, H.K., Lee, K., Hong, Y., Cho, J.H., Choi, J.W., Lee, J.I., Suh, Y.L., Ku, B.M., Eum, H.H., et al. (2020). Single-cell RNA sequencing demonstrates the molecular and cellular reprogramming of metastatic lung adenocarcinoma. Nat. Commun. *11*, 2285. https://doi.org/10.1038/s41467-020-16164-1.

Lai, G.G.Y., Lim, T.H., Lim, J., Liew, P.J.R., Kwang, X.L., Nahar, R., Aung, Z.W., Takano, A., Lee, Y.Y., Lau, D.P.X., et al. (2019). Clonal MET amplification as a determinant of tyrosine kinase inhibitor resistance in epidermal growth factor receptor-mutant non-small-cell lung cancer. J. Clin. Oncol. *37*, 876–884. https://doi.org/10.1200/JCO.18.00177.

Lambrechts, D., Wauters, E., Boeckx, B., Aibar, S., Nittner, D., Burton, O., Bassez, A., Decaluwé, H., Pircher, A., Van den Eynde, K., et al. (2018). Phenotype molding of stromal cells in the lung tumor microenvironment. Nat. Med. *24*, 1277–1289. https://doi.org/10.1038/s41591-018-0096-5.

Lee, J.K., Shin, J.Y., Kim, S., Lee, S., Park, C., Kim, J.Y., Koh, Y., Keam, B., Min, H.S., Kim, T.M., et al. (2013). Primary resistance to epidermal growth factor receptor (EGFR) tyrosine kinase inhibitors (TKIs) in patients with non-small-cell lung cancer harboring TKI-sensitive EGFR mutations: an exploratory study. Ann. Oncol. *24*, 2080–2087. https://doi.org/10.1093/annonc/mdt127.

Leonetti, A., Sharma, S., Minari, R., Perego, P., Giovannetti, E., and Tiseo, M. (2019). Resistance mechanisms to osimertinib in EGFR-mutated non-small cell lung cancer. Br. J. Cancer *121*, 725–737. https://doi.org/10.1038/s41416-019-0573-8.

Li, H., van der Leun, A.M., Yofe, I., Lubling, Y., Gelbard-Solodkin, D., van Akkooi, A.C.J., van den Braber, M., Rozeman, E.A., Haanen, J.B.A.G., Blank, C.U., et al. (2019). Dysfunctional CD8 T cells form a proliferative, dynamically regulated compartment within human melanoma. Cell *176*, 775–789.e18. https://doi.org/10.1016/j.cell.2018.11.043.

Love, M.I., Huber, W., and Anders, S. (2014). Moderated estimation of fold change and dispersion for RNA-seq data with DESeq2. Genome Biol. *15*, 550. https://doi.org/10.1186/s13059-014-0550-8.

Maynard, A., McCoach, C.E., Rotow, J.K., Harris, L., Haderk, F., Kerr, D.L., Yu, E.A., Schenk, E.L., Tan, W., Zee, A., et al. (2020). Therapy-induced evolution of human lung cancer revealed by single-cell RNA sequencing. Cell *182*, 1232–1251.e22. https://doi.org/10.1016/j.cell.2020.07.017.

Mazieres, J., Antonia, T., Daste, G., Muro-Cacho, C., Berchery, D., Tillement, V., Pradines, A., Sebti, S., and Favre, G. (2004). Loss of RhoB expression in human lung cancer progression. Clin. Cancer Res. *10*, 2742–2750. https://doi.org/10.1158/1078-0432.ccr-03-0149.

Mehrfeld, C., Zenner, S., Kornek, M., and Lukacs-Kornek, V. (2018). The contribution of non-professional antigen-presenting cells to immunity and tolerance in the liver. Front. Immunol. *9*, 635. https://doi.org/10.3389/fimmu.2018.00635.

Patel, A.P., Tirosh, I., Trombetta, J.J., Shalek, A.K., Gillespie, S.M., Wakimoto, H., Cahill, D.P., Nahed, B.V., Curry, W.T., Martuza, R.L., et al. (2014). Single-cell RNA-seq highlights intratumoral heterogeneity in primary glioblastoma. Science *344*, 1396–1401. https://doi.org/10.1126/science.1254257.

Peng, R., Jiang, B., Ma, J., Ma, Z., Wan, X., Liu, H., Chen, Z., Cheng, Q., and Chen, R. (2013). Forced downregulation of RACK1 inhibits glioma development by suppressing Src/Akt signaling activity. Oncol. Rep. *30*, 2195–2202. https://doi.org/10.3892/or.2013.2723.

Plasschaert, L.W., Žilionis, R., Choo-Wing, R., Savova, V., Knehr, J., Roma, G., Klein, A.M., and Jaffe, A.B. (2018). A single-cell atlas of the airway epithelium reveals the CFTR-rich pulmonary ionocyte. Nature *560*, 377–381. https://doi.org/10.1038/s41586-018-0394-6.

Pollack, B.P., Sapkota, B., and Cartee, T.V. (2011). Epidermal growth factor receptor inhibition augments the expression of MHC class I and II genes. Clin. Cancer Res. *17*, 4400–4413. https://doi.org/10.1158/1078-0432.CCR-10-3283.

Qin, S., Jiang, J., Lu, Y., Nice, E.C., Huang, C., Zhang, J., and He, W. (2020). Emerging role of tumor cell plasticity in modifying therapeutic response. Signal Transduct. Target. Ther. *5*, 228. https://doi.org/10.1038/s41392-020-00313-5.

Riely, G.J., Pao, W., Pham, D., Li, A.R., Rizvi, N., Venkatraman, E.S., Zakowski, M.F., Kris, M.G., Ladanyi, M., and Miller, V.A. (2006). Clinical course of patients with non-small cell lung cancer and epidermal growth factor receptor exon 19 and exon 21 mutations treated with gefitinib or erlotinib. Clin. Cancer Res. *12*, 839–844. https://doi.org/10.1158/1078-0432.CCR-05-1846.

Sharma, S.V., Bell, D.W., Settleman, J., and Haber, D.A. (2007). Epidermal growth factor

receptor mutations in lung cancer. Nat. Rev. Cancer *7*, 169–181. https://doi.org/10.1038/nrc2088.

Steimle, V., Siegrist, C.A., Mottet, A., Lisowska-Grospierre, B., and Mach, B. (1994). Regulation of MHC class II expression by interferon-gamma mediated by the transactivator gene CIITA. Science *265*, 106–109. https://doi.org/10.1126/science.8016643.

Su, S., Dong, Z.Y., Xie, Z., Yan, L.X., Li, Y.F., Su, J., Liu, S.Y., Yin, K., Chen, R.L., Huang, S.M., et al. (2018). Strong programmed death ligand 1 expression predicts poor response and de novo resistance to EGFR tyrosine kinase inhibitors among NSCLC patients with EGFR mutation. J. Thorac. Oncol. *13*, 1668–1675. https://doi.org/10.1016/j.jtho.2018.07.016.

Swiecki, M., and Colonna, M. (2015). The multifaceted biology of plasmacytoid dendritic cells. Nat. Rev. Immunol. *15*, 471–485. https://doi.org/10.1038/nri3865.

Takashima, Y., Sakakibara-Konishi, J., Hatanaka, Y., Hatanaka, K.C., Ohhara, Y., Oizumi, S., Hida, Y., Kaga, K., Kinoshita, I., Dosaka-Akita, H., et al. (2018). Clinicopathologic features and immune microenvironment of non-small-cell lung cancer with primary resistance to epidermal growth factor receptor tyrosine kinase inhibitors. Clin. Lung Cancer *19*, 352–359.e1. https://doi.org/10.1016/j.cllc.2018.02.004.

Wind, S., Schnell, D., Ebner, T., Freiwald, M., and Stopfer, P. (2017). Clinical pharmacokinetics and pharmacodynamics of afatinib. Clin. Pharmacokinet. *56*, 235–250. https://doi.org/10.1007/s40262-016-0440-1.

Wolock, S.L., Lopez, R., and Klein, A.M. (2019). Scrublet: computational identification of cell doublets in single-cell transcriptomic data. Cell Syst. *8*, 281–291.e9. https://doi.org/10.1016/j.cels.2018.11.005.

Wosen, J.E., Mukhopadhyay, D., Macaubas, C., and Mellins, E.D. (2018). Epithelial MHC class II expression and its role in antigen presentation in the gastrointestinal and respiratory tracts. Front. Immunol. *9*, 2144. https://doi.org/10.3389/fimmu.2018.02144.

Yao, J., Caballero, O.L., Yung, W.K.A., Weinstein, J.N., Riggins, G.J., Strausberg, R.L., and Zhao, Q. (2014). Tumor subtype-specific cancer-testis antigens as potential biomarkers and immunotherapeutic targets for cancers. Cancer Immunol. Res. *2*, 371–379. https://doi.org/10.1158/2326-6066.CIR-13-0088.

Ye, Y., Gaugler, B., Mohty, M., and Malard, F. (2020). Plasmacytoid dendritic cell biology and its role in immune-mediated diseases. Clin. Transl. Immunology *9*, e1139. https://doi.org/10.1002/cti2.1139.

Zhong, J., Li, L., Wang, Z., Bai, H., Gai, F., Duan, J., Zhao, J., Zhuo, M., Wang, Y., Wang, S., et al. (2017). Potential resistance mechanisms revealed by targeted sequencing from lung adenocarcinoma patients with primary resistance to epidermal growth factor receptor (EGFR) tyrosine kinase inhibitors (TKIs). J. Thorac. Oncol. *12*, 1766–1778. https://doi.org/10.1016/j.jtho.2017.07.032.

STAR★METHODS

KEY RESOURCES TABLE

REAGENT or RESOURCE	SOURCE	IDENTIFIER
Antibodies		
Recombinant Anti-HLA-DPB1 antibody [EPR11226]	Abcam	Cat# ab157210; RRID: AB_2827533
Recombinant Anti-HLA-DQA1 antibody [EPR7300]	Abcam	Cat# ab128959; RRID: AB_11145506
HLA-DRB1 antibody [N1C3]	GeneTex	Cat# GTX104919; RRID: AB_10616679
Cytokeratin Pan Antibody Cocktail	Thermo Scientific	Cat# MA5-13203; RRID: AB_10942225
Purified Mouse Anti-Human CD45	BD Bioscience	Cat# 555480; RRID: AB_395872
Recombinant Anti-HLA-DR antibody [TAL 1B5]	Abcam	Cat# ab20181; RRID: AB_445401
Anti-CSAG1 antibody	Abcam	Cat# ab238872
CIITA Antibody	Novus Biologicals	Cat# NBP2-59072
MAGEA3 Monoclonal Antibody (OTI1G9)	Thermo Scientific	Cat# MA5-26486; RRID: AB_2724631
EpCAM Monoclonal Antibody (VU-1D9), FITC	Thermo Scientific	Cat# MA1-10197
BV421 Mouse Anti-Human CD3	BD Bioscience	Cat# 563798
Alexa Fluor® 488 anti-human CD326 (EpCAM) Antibody	BioLegend	Cat# 324210; RRID: AB_756084
Alexa Fluor® 488 Mouse IgG2b, κ Isotype Ctrl Antibody	BioLegend	Cat# 400329
Pan Cytokeratin Monoclonal Antibody (AE1/AE3), Alexa Fluor™ 488	eBioscience	Cat# 53-9003-82; RRID: AB_1834350
Mouse IgG1 Alexa Fluor® 488-conjugated Antibody	R&D System	Cat# IC002G; RRID: AB_10718385
CD45 monoclonal Antibody(HI30)eFluor 450	eBioscience	Cat# 48-0459-42; RRID: AB_2016677
Mouse IgG1 kappa Isotype control eFluor 450	eBioscience	Cat# 48-4714-82; RRID: AB_1271992
PE anti-human IFN-γ Antibody	BioLegend	Cat# 506507; RRID: AB_315440
PE Mouse IgG1, κ Isotype Ctrl (ICFC) Antibody	BioLegend	Cat# 400140; RRID: AB_493443
APC Mouse Anti-Human CD45	BD Bioscience	Cat# 560973; RRID: AB_10565969
HLA-DR Monoclonal Antibody (LN3), APC	eBioscience	Cat# 17-9956-42;RRID: AB_10670347
Mouse IgG2b kappa Isotype Control (eBMG2b), APC	eBioscience	Cat# 17-4732-81; RRID: AB_763656
Chemicals, peptides, and recombinant proteins		
Human TruStain FcX™ (Fc Receptor Blocking Solution)	BioLegend	Cat# 422302;RRID: AB_2818986
Stain Buffer (BSA)	BD Bioscience	Cat# 554657;RRID: AB_2869007
eBioscience™ Intracellular Fixation & Permeabilization Buffer Set	eBioscience	Cat# 88-8824-00
Protein Transport Inhibitor	BD Bioscience	Cat# 554724;RRID: AB_2869012
Phorbol 12-myristate 13-acetate (PMA)	Sigma-Aldrich	Cat# P8139
Ionomycin calcium salt from Streptomyces conglobatus	Sigma-Aldrich	Cat# I0634
Deposited data		
Single-cell RNA sequencing data	Sequence Read Archive	PRJNA668853

(*Continued on next page*)

Continued

REAGENT or RESOURCE	SOURCE	IDENTIFIER
Software and algorithms		
CellRanger	10x Genomics	https://support.10xgenomics.com/single-cell-gene-expression/software/downloads/
Scrublet	GitHub	https://github.com/AllonKleinLab/scrublet
Seurat	GitHub	https://github.com/satijalab/seurat
DESeq2	Bioconductor	https://bioconductor.org/packages/DESeq2
EnrichR	CRAN	https://cran.r-project.org/web/packages/enrichR/
inferCNV	GitHub	https://github.com/broadinstitute/inferCNV/
Prism GraphPad 7	GraphPad Software	https://www.graphpad.com/scientific-software/prism/
ggplot2	CRAN	https://cran.r-project.org/web/packages/ggplot2/
Pheatmap	CRAN	https://cran.r-project.org/web/packages/pheatmap/
R project for statistical computing	R Core Team	https://www.r-project.org
Python Programming Language	Python	https://www.python.org
Source code	This paper	https://github.com/CompbioLabUnist/EGFR-TKI-scRNAseq

RESOURCE AVAILABILITY

Lead contact

Further information and requests for resources and reagents should be directed to and will be fulfilled by the lead contact, Se-Hoon Lee (shlee119@skku.edu).

Materials availability

This study did not generate new unique reagents.

Data and code availability

Single-cell RNA-seq data have been deposited at Sequence Read Archive (SRA: PRJNA668853) and are publicly available as of the date of publication. Accession numbers are listed in the key resources table. Code is available from a github repository (https://github.com/CompbioLabUnist/EGFR-TKI-scRNAseq). Any additional information required to reanalyze the data reported in this paper is available from the lead contact upon request.

EXPERIMENTAL MODEL AND SUBJECT DETAILS

Collection and preparation of pleural effusion samples of NSCLC patients

Samples were collected after receiving consent and approval from the Institutional Review Board (IRB No. 2010-04-039 and IRB No. 2019-05-049) at Samsung Medical Center. The collected pleural effusions of NSCLC patients were centrifuged at 1,500 rpm for 15 min, after which the samples were washed with PBS. Thereafter, samples were digested using mixtures of collagenase type II (LS004174; Worthington Biochemical Corporation, Lakewood, NJ, USA) plus deoxyribonuclease I (LS002139; Worthington Biochemical Corporation) for 15 min at 37°C. Afterward, digested cells were passed through a 40-μm pore filter and subjected to RBC lysis for 10 min at room temperature. After washing with PBS, cells on the plate were incubated for 15 min in a CO_2 incubator. Only floating cells on the plate were collected, while adherent cells were excluded. The counted cells were then stocked and frozen. Except for one surgical sample, eight samples were thawed for library preparation and sequenced using 10x Chromium Single Cell Gene Expression Solution v2 (10x Genomics, Pleasanton, CA, USA) according to the manufacturer's protocols. Six out of nine study patients were females, and additional clinical information for the patients are provided in Table S1.

METHOD DETAILS

scRNA-seq data processing

Sequencing results were demultiplexed and converted to the FASTQ format using Illumina bcl2fastq software (Illumina, San Diego, CA, USA). The Cell Ranger Single-Cell Software Suite (https://support.10xgenomics.com/single-cell-gene-expression/software/pipelines/latest/what-is-cell-ranger, version 3.0.2) was used to perform sample demultiplexing, barcode processing, and single-cell 3′ gene counting. The cDNA insert was aligned to the hg19 reference genome. Only confidently mapped, non-PCR duplicates with valid barcodes and unique molecular identifiers were used to generate the gene-barcode matrix. We applied Scrublet (Wolock et al., 2019) to remove doublets that occur when two or more cells enter the same microfluidic droplet. Further analysis, including quality filtering, identifying highly variable genes, dimensionality reduction, standard unsupervised clustering algorithms, and the discovery of differentially expressed genes (DE-Gs), was performed using the Seurat R package (version 3.1.4) (Butler et al., 2018). To exclude low-quality cells, we used QC covariates such as counts per cell, number of genes per cell, and mitochondrial gene ratio per cell. Because the distribution of these QC covariates differs for each sample (Plasschaert et al., 2018), we determined different thresholds for each sample. After removing unwanted cells from the dataset, we normalized the data by the total expression, multiplied by a scale factor of 10,000 using the ScaleData function. We used FindVariableFeatures to identify highly variable genes and then performed PCA with the top 2,000 variable genes. Clusters were partitioned using FindClusters, and each cell was projected into a two-dimensional space using t-Stochastic Neighbor Embedding. DE-Gs in each cluster were calculated using the FindMarkers function. We integrated two different scRNA-seq datasets using Seurat canonical correlation analysis alignment.

Correlation analysis of epithelial cells for infer cellular plasticity

To infer the cellular plasticity of epithelial cells, we performed a correlation analysis with previously reported epithelial cell types (Deprez et al., 2020). We averaged the gene expression of cells of each cell type, and then we analyzed the correlation between the gene expression values for each defined cell type and the gene expression values of MPE-derived cells at the cellular level. Each cell was assigned the cell type with the highest Pearson correlation coefficient, and cell types were restricted to the epithelial cell type.

Differential gene expression analysis of pseudo-bulks

We combined all the cells from each sample to create pseudo-bulk samples. DE-Gs were identified using the DESeq2 R package (version 1.26.0) (Love et al., 2014) based on the average expression level (mean CPM) of each cell. Each DEG was filtered using abs (fold change) > 1 and p value < 0.05. We used EnrichR (Chen et al., 2013) to analyze the enrichment of biological process ontology.

Copy number variation analysis in scRNA-seq

Copy number variation (CNV) in each cell was estimated using the inferCNV R package (version 1.2.1) (Patel et al., 2014). Each CNV level was estimated using relative expression values with a sliding window of 100 genes based on the genomic location of the genes. All assays were analyzed using the default option, and the CNV of epithelial cells was estimated with reference to myeloid cells.

Cell viability test

In the cell viability test, cells were equally distributed into 96-well plates with 7,000 cells/well. Thereafter, cells were separately exposed to TKI drugs (gefitinib, erlotinib, osimertinib, and afatinib) in 1/4 and seven-point serial dilution doses from 4 nM to 20 μM for 72 h. Subsequently, CellTiter-Glo Luminescent Cell Viability Assay reagents (G7572; Promega, Madison, WI, USA) were added to each well at a 1:1 ratio with media volume and shaken gently. The plates were incubated at room temperature for 15–30 min, and cell viability was determined using a Mithras LB940 Multimode Microplate Reader (Berthold Technologies GmbH & Co. KG, Bad Wildbad, Germany) according to the manufacturer's protocols.

Immunohistochemistry staining

FFPE tumor sections were dewaxed in xylene and ethanol and submerged into ER1 buffer (pH 6.0) for 20 min at 100°C in a Bond-RX Multiplex IHC Stainer (Leica Biosystem, Melbourne, Australia) to retrieve the antigens, followed by incubation in endogenous peroxidase for 10 min. Anti-HLA-DPB1 antibody (Abcam, Cambridge, UK) was diluted at 1:1,000 and incubated with Bond-RX autoimmunostainer for 15 min.

For the HLA-DRB1 (IHC) test, we diluted the anti-HLA-DRB1 antibody (GeneTex, Irvine, CA, USA) to 1:2,000 and incubated it with Bond-RX autoimmunostainer for 15 min. For the HLA-DQA1 test, we diluted the anti-HLA-DQA1 antibody (Abcam) to 1:200 and incubated it with Bond-RX autoimmunostainer for 15 min. Subsequently, the immunostained slides were evaluated by an experienced pathologist. IHC scores were assessed by both staining intensity and the percentage of positive tumor cells. The staining intensity was graded from 0 to 3 (0, no staining; 1, weak staining; 2, moderate staining; and 3, strong staining) by relative degree within each antibody. The percentage of positive staining cells was recorded from 0 to 100%. In addition, we evaluated the quality of the IHC test depending on the staining of immune cells (internal control).

Multiplex immunofluorescence

After fixing with 4% paraformaldehyde for 30 min, MPE cells were embedded with pre-warmed HistoGel (Thermo Scientific, MI, USA) according to the manufacturer's instructions by using cryomolds (Disposable vinyl specimen molds 10 × 10 × 5 mm, Tissue-Tek, Sakura Finetek, Torrance, CA, USA). Followed by placing on ice until the Histogel is solidified, cell block was wrapped with a filter paper and put into tissue cassette for further fixation and routine tissue processing procedures of paraffin embedding. Prior to staining, all cell block slides were deparaffinized on the Leica BOND RX automated immunostainer (Leica Microsystems, Milton Keynes, UK) by baking for 30 min at 60°C, soaking in BOND Dewax Solution at 72°C and then rehydrating in ethanol. Followed by heat-induced epitope retrieval (HIER) pretreatments applied at 95°C using citrate-based Epitope Retrieval (ER) Solution (pH 6.0, Leica Biosystems), the tyramide signal amplification (TSA)-based Opal method was used for multiplex immunofluorescence (mIF) staining (Opal Polaris 7-Color Automation IHC Kit; Akoya Biosciences, Marlborough, MA, USA). mIF was performed using the following antibodies: anti-EpCAM (Thermo Scientific, #MA1-10195), anti-CD45 (BD Pharmingen, #555480), anti-HLA-DR (Abcam, #ab20181), anti-MAGEA3 (Thermo Fisher Scientific, #MA5-26468), anti-CIITA (Novus biological, #NBP2-59072) and anti-CSAG-1 (Abcam, #ab238872). The Opal fluorophores were used to visualize each biomarker: Opal 690 (EpCAM), Opal 780 (HLA-DR), Opal 620 (CIITA), Opal 570 (CSAG1), Opal 520 (MAGEA3), and Opal 480 (CD45). Slides were incubated with DAPI as counterstain and coverslipped with Prolong antifade mountant (Thermo Fisher Scientific). Whole slides were scanned using the Vectra-Polaris 3.0.3, a multispectral imaging system (Akoya Biosciences), at a low magnification of 10×. And, quantification analysis and image capture were performed with In-Form 2.6.0. and Phenochart 1.0.9 image viewer software (Akoya Biosciences).

Flow cytometry

MPE cells were incubated with Human TruStain FcX™ (Fc Receptor Blocking Solution, BioLegend) for 10 min at room temperature, and labeled for surface markers with EpCAM Monoclonal Antibody (VU-1D9, Thermo Scientific), HLA-DR Monoclonal Antibody (LN3, eBioscience), BV421 Mouse Anti-Human CD3 Antibody (SK7, BD Bioscience), and CD45 monoclonal Antibody (HI30, eBioscience). Then, they were fixed and permeabilized by using eBioscience™ Intracellular Fixation & Permeabilization Buffer Set for intracellular staining with Pan Cytokeratin Monoclonal Antibody (AE1/AE3, eBioscience) and PE anti-human IFN-γ Antibody (B27, BioLegend). Stained cells were analyzed with BD FACSVerse™ flow cytometer and BD FACSuite™ software (BD biosciences).

MPE-derived organoid culture

Collected pleural effusion from T EGFR-TKI sensitive or EGFR-TKI resistant patients was centrifuged at 1500g for 15 min and the pellet was incubated with enzyme mixture containing collagenase II (5 mg/mL, Worthington) and DNase I (1.7 mg/mL, Worthington) for 10 min at 37°C. After washing with phosphate buffered saline, cells were filtered with 40 μm cell strainer and red blood cells were lysed for 10 min at room temperature. Washed cells were suspended in ACL4 medium (Hyclone) containing EGF (10 ng/mL, PeproTech), FGF (10 ng/mL, PeproTech), IGF (20 ng/mL, PeproTech), A83-01 (5 μM, Sigma), 2.5% heat-inactivated fetal bovine serum (Gibco) and 1x Antibiotic-Antimycotic (Gibco). Counted MPE cells (0.5-1x10^6/100 μL media) were mixed with matrigel (Corning) in a 1:1 ratio, plated and incubated at 37°C for several days with media change every 3–4 days. MPE organoids were collected by removing matrigel with cell recovery solution (Corning), and lysed for western blot to examine the expression of HLA class II.

Analysis of clinical validation cohort

Progression-free survival (PFS) was calculated from the date of TKI treatment to the date of disease progression or death, and the hazard ratio (HR) was computed using a log rank of survival calculations. The patient group was classified as TKI resistant if disease progression occurred within 90 days and TKI sensitive if TKI treatment continued for more than 180 days. Cases where the IHC score is greater than the median value were defined as High, and those where the IHC score was less than the median value were defined as Low, and Kaplan–Meier calculations were performed. Non-parametric Non-parametric data and IHC score were analyzed using the Wilcoxon rank-sum test. R software and GraphPad Prism Ver8.0 were used for the analysis, and statistical significance was considered at $p < 0.05$.

QUANTIFICATION AND STATISTICAL ANALYSIS

For all statistical test to comparing the difference in the proportion of cell types between the two groups, wilcoxon rank-sum test was used to evaluate the p value. Statistical analysis was implemented using R and the statistical details of analysis can be found in the results and figures legends.